Structural Dynamics of Hydrated Phospholipid Surfaces Probed by Ultrafast 2D Spectroscopy of Phosphate Vibrations

ARTICLE *in* JOURNAL OF PHYSICAL CHEMISTRY LETTERS · JANUARY 2014

Impact Factor: 7.46 · DOI: 10.1021/jz402493b

3 AUTHORS, INCLUDING:

Rene Costard
Max-Born-Institut für Nichtlineare Optik und…
16 PUBLICATIONS **102** CITATIONS
SEE PROFILE

Ismael A Heisler
University of East Anglia
47 PUBLICATIONS **536** CITATIONS
SEE PROFILE

THE JOURNAL OF PHYSICAL CHEMISTRY Letters

Letter

pubs.acs.org/JPCL

Structural Dynamics of Hydrated Phospholipid Surfaces Probed by Ultrafast 2D Spectroscopy of Phosphate Vibrations

Rene Costard, Ismael A. Heisler, and Thomas Elsaesser*

Max-Born-Institut für Nichtlineare Optik und Kurzzeitspektroskopie, Max-Born-Strasse 2 a, 12489 Berlin, Germany

Supporting Information

ABSTRACT: The properties of biomembranes depend in a decisive way on interactions of phospholipids with hydrating water molecules. To map structural dynamics of a phospholipid−water interface on the length and time scale of molecular motions, we introduce the phospholipid symmetric and asymmetric phosphate stretch vibrations as probes of interfacial hydrogen bonds and electrostatic interactions. The first two-dimensional infrared spectra of such modes and a line shape analysis by density matrix theory reveal two distinct structural dynamics components; the first 300 fs contribution is related to spatial fluctuations of charged phospholipid head groups with additional water contributions at high hydration levels; the second accounts for water−phosphate hydrogen bonds persisting longer than 10 ps. Our results reveal a relatively rigid hydration shell around phosphate groups, a behavior relevant for numerous biomolecular systems.

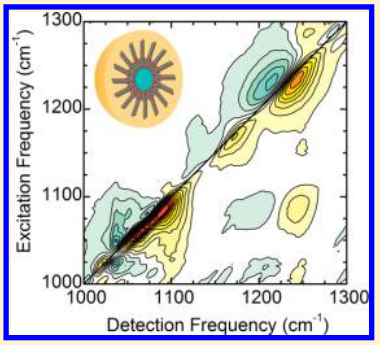

SECTION: Biophysical Chemistry and Biomolecules

Interactions of phosphate groups with their aqueous environment have a decisive impact on biomolecular structure and function. The hydration degree of phosphate groups in the backbone of DNA is essential for the double-helix structure, undergoing a transition from a B- to an A-helix geometry at reduced water levels.[1] In phospholipids, the building blocks of biological membranes, interfacial water hydrates the head groups, in this way both shielding electric fields and stabilizing the membrane geometry.[2−4] The primary hydration sites of phospholipids are their phosphate and carbonyl groups (see Figure 1a), where water molecules are able to attach by hydrogen bonding.[2−13] The phosphate groups at the membrane surface are locally hydrated by up to six water molecules, interacting via both local hydrogen bonds and electric polarization forces. The carbonyl groups are hydrated by individual water molecules, while the choline group of phospholipids is embedded in a clathrate-type structure consisting of about 20 water molecules within a radial distance of 0.6 nm. Here, the water oxygens of the first layer are oriented toward the N^+ center ion.[7,11] In addition to local hydrogen bonds, there are strong electric fields at the water−phospholipid interface that originate mainly from the large head group dipole moments on the order of 20 D.[5,8,10,12] Such fields lead to a spatial alignment of the head groups and interfacial water molecules, the latter partly compensating for the head group dipoles.

In the present work, we focus on the dynamics of the phospholipid−water interface. Experimental studies, molecular structure calculations, and molecular dynamics (MD) simulations have shown that thermally activated motions and fluctuations of phospholipid membranes cover a very wide time range from picoseconds to seconds, directly affecting the electrostatic potential, the electronic charge distribution, and the spatial arrangement of water molecules interacting with phospholipids.[8,10,13−16] The calculated time correlation functions of hydrogen bond lifetimes, residence times of water molecules in the first hydration layer, and water reorientation strongly suggest that the lifetimes of phosphate−water hydrogen bonds are longer than the ∼1 ps lifetime of hydrogen bonds in bulk water. The calculated lifetimes, however, spread between a few and tens of picoseconds. The exchange of water molecules between the interfacial and second water layer is considered a process happening on a 30−50 ps time scale. The correlation functions calculated for the angular reorientation of water molecules display multiexponential decays with a fast subpicosecond component, followed by one or several components extending to tens of picoseconds. Direct experimental information on the fastest processes affecting the structure of the phospholipid−water interface has remained very limited.[6,17]

Vibrational spectroscopy in the femto- to picosecond time domain allows for mapping structural dynamics of hydrated phospholipids and for characterizing phospholipid−water interactions on the time scale of molecular motions and hydrogen bond dynamics. So far, femtosecond infrared pump−probe experiments have focused on dynamics of OH or OD stretch excitations of water mainly to address water structure, reorientation, and energy dissipation.[18−21] A major drawback of this approach consists of the spatial averaging over all water environments, that is, a selective observation of interfacial water at biologically relevant high hydration levels is impossible. Nevertheless, results for low hydration levels point to a slowing

Received: November 18, 2013
Accepted: January 21, 2014

   dx.doi.org/10.1021/jz402493b | J. Phys. Chem. Lett. 2014, 5, 506−511

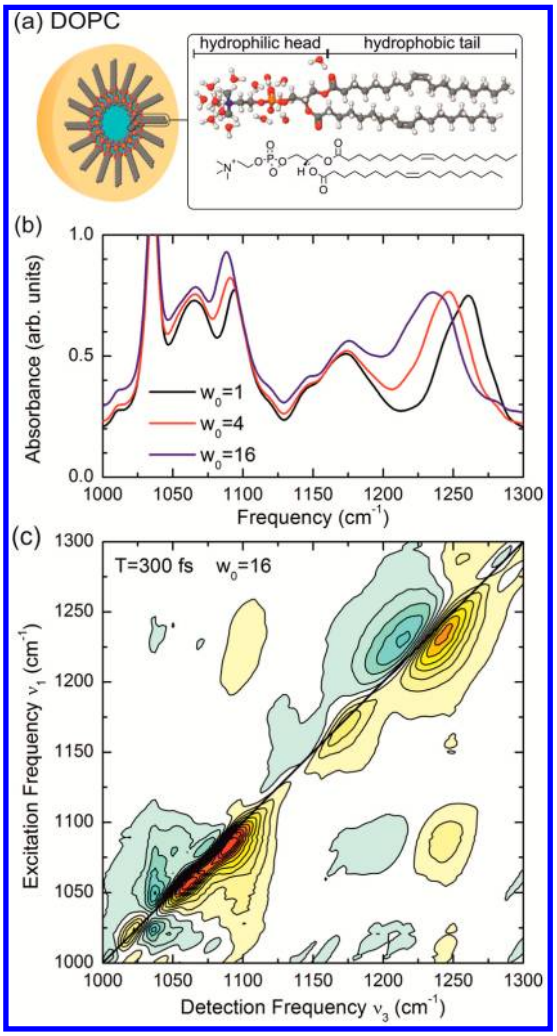

Figure 1. (a) Schematic of a reverse micelle consisting of DOPC phospholipids (small blue spheres: phosphate groups; orange spheres: choline groups) and a water pool (light blue) inside. (Right) Molecular structure of DOPC. The upper scheme includes hydrating H_2O molecules. (b) Infrared absorption of DOPC reverse micelles for different levels of hydration. The asymmetric $(PO_2)^-$ stretch vibration $\nu_{AS}(PO_2)^-$ at around 1250 cm^{-1} displays a pronounced red shift with increasing hydration. The red shift of the symmetric $(PO_2)^-$ stretch vibration $\nu_S(PO_2)^-$ at around 1095 cm^{-1} is smaller. The band at 1065 cm^{-1} is due to the symmetric CO−O−C stretch and the C−O−P stretch vibration, while the band at 1175 cm^{-1} represents the asymmetric CO−O−C stretch absorption. The narrow absorption band at 1035 cm^{-1} is caused by the solvent benzene. (c) 2D spectrum of DOPC reverse micelles at a hydration level $w_0 = 16$. The absorptive 2D signal is plotted as a function of the excitation frequency ν_1 and the detection frequency ν_3. The data were taken for a population time of T = 300 fs. The signal amplitudes change by 10% between neighboring contour lines.

down of water reorientation at the interface compared to bulk water.[19,22,23]

Here, we introduce the phosphate $(PO_2)^-$ stretching vibrations of the phospholipid head groups as vibrational probes of interfacial dynamics in a wide range of hydration. By measuring the first 2D infrared spectra of the symmetric and asymmetric $(PO_2)^-$ stretch vibrations, we identify the time scales of interfacial phospholipid and water dynamics. We study such processes in phospholipid reverse micelles, a basic model system that displays a well-defined geometry and allows for varying of the hydration level in a controlled way. Our results reveal a 300 fs component in the frequency−time correlation function (tcf), which is due to phospholipid fluctuations and, at higher hydration levels, orientational fluctuations of water molecules. This fast decay is followed by a slow correlation decay for which we determine a minimum decay time of 10 ps. This value sets a lower limit for the hydrogen bond lifetime and water residence time in the first hydration layer, displaying an essentially rigid structure into the picosecond time range.

The phospholipid system studied here consists of dioleoylphosphatidylcholine (DOPC) reverse micelles[24] (Figure 1a), which contain H_2O and are dissolved in benzene (concentration of 0.25 M). Details of sample preparation are presented in the Supporting Information (SI). The hydration level is varied from a 1:1 ratio of water to DOPC molecules ($w_0 = 1$) up to a 16:1 ratio ($w_0 = 16$). Figure 1b shows the infrared absorption spectrum of the reverse micelles in the range of the symmetric ($\nu_S(PO_2)^-$) and asymmetric ($\nu_{AS}(PO_2)^-$) stretching vibrations of the DOPC phosphate groups.[24] With increasing hydration level, both bands undergo a spectral red shift that is substantially stronger for $\nu_{AS}(PO_2)^-$ than that for $\nu_S(PO_2)^-$.[24,25] This fact makes the phosphate stretch vibrations sensitive probes of interfacial water as changes in the number of local hydrogen bonds and/or fluctuations of the hydrating water structure affect both the linear infrared absorption and the nonlinear 2D spectra. The $v = 1$ lifetime of $\nu_{AS}(PO_2)^-$ has a value of 300 fs, which is independent from w_0.[24] The much longer $v = 1$ lifetime of $\nu_S(PO_2)^-$ has a value of 1.5 ps at $w_0 = 1$ and 1.0 ps at $w_0 = 16$ (cf. Figure S1, SI).

We implemented the first femtosecond 2D infrared experiment[26,27] covering a spectral range from 1000 to 1300 cm^{-1} in order to measure 2D spectra of $\nu_S(PO_2)^-$ and $\nu_{AS}(PO_2)^-$. In Figure 1c, we present an absorptive 2D spectrum, that is, the sum of the rephasing and nonrephasing third-order signal[28] plotted as a function of the excitation frequency ν_1 and the detection frequency ν_3, both covering the range from 1000 to 1300 cm^{-1}. The spectrum was recorded at a population time of T = 300 fs (delay between the second and third pulse) for a DOPC reverse micelle sample of $w_0 = 16$. The positive diagonal peaks (yellow−red contours) are due to the $v = 0$ to 1 transitions of $\nu_{AS}(PO_2)^-$ at 1240 cm^{-1}, the asymmetric CO−O−C stretch vibration at 1175 cm^{-1}, $\nu_S(PO_2)^-$ at 1095 cm^{-1}, and a superposition of the symmetric CO−O−C and C−O−P stretch vibrations at 1068 cm^{-1}.[29]

All diagonal peaks in the 2D spectrum display a shape elongated along the diagonal, pointing to a pronounced inhomogeneous broadening. The $v = 1$ to 2 transitions of the different vibrations cause negative peaks (blue contours) that occur at smaller detection frequencies ν_3 because of the anharmonicity of the oscillators and display a diagonal and antidiagonal spectral width similar to that of the $v = 0$ to 1 component. There are pronounced positive cross peaks between $\nu_{AS}(PO_2)^-$ and $\nu_S(PO_2)^-$ at (ν_1,ν_3) = (1240,1095) cm^{-1} and at (ν_1,ν_3) = (1095,1240) cm^{-1}, giving evidence of the coupling of the two phosphate stretching modes. Cross peak features are also found between $\nu_S(PO_2)^-$ and the modes at ν_3 = 1060 cm^{-1}.

The amplitude of the positive and negative peaks in the 2D spectra decreases for longer population times due to the relaxation of the $v = 1$ state with a 300 fs lifetime for $\nu_{AS}(PO_2)^-$, independently of hydration level, and a 1.0−1.5 ps lifetime for $\nu_S(PO_2)^-$ for high and low hydration level, respectively.

dx.doi.org/10.1021/jz402493b | J. Phys. Chem. Lett. 2014, 5, 506−511

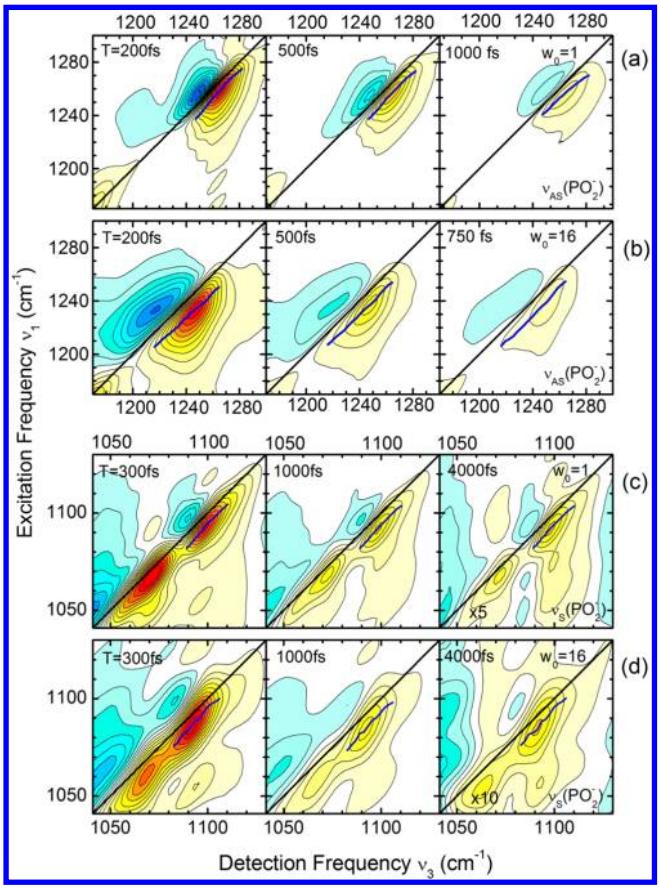

Figure 2. Two-dimensional (2D) infrared spectra of (a,b) the asymmetric $(\nu_{AS}(PO_2)^-)$ and (c,d) the symmetric $(\nu_S(PO_2)^-)$ phosphate stretching vibrations of DOPC. The diagonal peak of $\nu_S(PO_2)^-$ is located at around 1095 cm^{-1}, while the diagonal peak at 1060 cm^{-1} is due to the symmetric CO−O−C and the C−O−P vibration of DOPC. Spectra are shown for hydration levels $w_0 = 1$ and 16 and different population times T. The absorptive third-order nonlinear signal is plotted as a function of the excitation frequency ν_1 and the detection frequency ν_3. Yellow−red contours represent (positive) signals due to the $\nu = 0$ to 1 transition of the vibrations, while blue contours represent negative signals from the $\nu = 1$ to 2 transitions. The signal amplitudes change by 10% between neighboring contour lines. The blue solid lines are center lines (CLs) derived from frequency cuts of the positive signal along ν_1 (fixed ν_3).

Pump−probe data and analysis of signal amplitudes of the 2D spectra are discussed in the SI.

In the following, we focus on the 2D lineshapes of $\nu_S(PO_2)^-$ and $\nu_{AS}(PO_2)^-$. Figure 2 shows absorptive 2D spectra of $\nu_{AS}(PO_2)^-$ for (a) $w_0 = 1$ and (b) $w_0 = 16$ for population times up to $T = 1000$ fs. At both hydration levels, one observes inhomogeneously broadened elliptic line shapes of the $\nu = 0$ to 1 and the $\nu = 1$ to 2 peaks, undergoing minor changes as a function of T. The 2D spectra for $w_0 = 16$ display a somewhat larger width along the antidiagonal than the $w_0 = 1$ spectra and, at $T = 1$ ps, a slight frequency upshift of their maximum on the diagonal $\nu_1 = \nu_3$. This frequency shift reflects vibrational relaxation processes, which are addressed in the SI. 2D spectra of $\nu_S(PO_2)^-$ at around 1090 cm^{-1} for population times up to $T = 4000$ fs are shown in Figure 2c ($w_0 = 1$) and Figure 2d ($w_0 = 16$), displaying minor changes of the 2D line shapes with increasing T. To illustrate this behavior in more detail, we present frequency slices of the 2D spectra for $\nu_S(PO_2)^-$ and $\nu_{AS}(PO_2)^-$ in Figure S2 (SI). In Figures S3 and S4 (SI), 2D spectra and frequency slices normalized to the maximum signal at each population time T are shown for comparison. For a first assessment of a potential reshaping of the 2D line shapes, we consider the center lines (CLs) shown as blue lines in Figure 2. For deriving CLs, the maximum intensity of spectral slices for a fixed detection frequency ν_3 was determined, and the spectral positions (ν_1,ν_3) of maxima in different slices were connected.[30] Within the experimental accuracy, the CL positions and slopes are unchanged with increasing population time T for both $\nu_{AS}(PO_2)^-$ and $\nu_S(PO_2)^-$ at both hydration levels, again pointing to minor spectral reshaping.

We performed a detailed and quantitative theoretical analysis of the 2D line shapes in order to extract information about the frequency−time correlation function (tcf), defined as $\langle\delta\nu(t)\delta\nu(0)\rangle$ of the two phosphate stretch vibrations. Here, $\delta\nu(t)$ is the deviation from the average phosphate stretch frequency at time t, and the brackets $\langle\rangle$ stand for the ensemble average of the correlation function. The tcf correlates frequency fluctuations at different instants in time and, thus, maps the underlying structural dynamics of the phospholipid−water system. The tcf is the key function necessary to calculate the line shapes of the linear infrared absorption (Figure 1b) and the 2D spectra (Figures 1c and 2).[27,31] Our analysis is based on the Kubo ansatz for the tcf, consisting of two exponential decay terms with amplitudes $\Delta\nu_1$ and $\Delta\nu_2$ and correlation times τ_{c1} and τ_{c2}

$$\langle\delta\nu(t)\delta\nu(0)\rangle = (\Delta\nu_1)^2 e^{-t/\tau_{c1}} + (\Delta\nu_2)^2 e^{-t/\tau_{c2}}$$

The form of this curve for different time constants is shown in the inset of Figure 3b (solid and dashed−dotted lines), and details of the theoretical treatment and calculated 2D spectra are presented in the SI.

In Figure 3, we compare spectral cuts through the $\nu = 0$ to 1 peaks of the measured 2D spectra parallel to the frequency diagonal $\nu_1 = \nu_3$ and antidiagonal cuts going through the $\nu = 0$ to 1 and $\nu = 1$ to 2 peaks (symbols) with calculated spectral slices (solid lines). The diagonal cuts in Figure 3a display the $\nu_S(PO_2)^-$ contribution at high detection frequencies, while the second component at low detection frequencies is due to the CO−O−C and C−O−P stretching vibrations. The 2D line shapes of $\nu_S(PO_2)^-$ and $\nu_{AS}(PO_2)^-$ measured at different hydration levels and population times T are well reproduced with correlation times of $\tau_{c1} = 300$ fs and $\tau_{c2} \rightarrow \infty$ and similar amplitudes for the two components. The vibrational anharmonicity $\Delta = \nu_{01} - \nu_{12}$ (where ν_{01} and ν_{12} are the frequencies of the $\nu = 0$ to 1 and $\nu = 1$ to 2 transitions) of both $\nu_S(PO_2)^-$ and $\nu_{AS}(PO_2)^-$ has a value of ~5 cm^{-1}. The exact values of the amplitudes are summarized in Table S1 of the SI. In Figure 3a, we compare diagonal cuts over an extended range of detection frequencies and population times T (symbols) with the cuts calculated for the $\nu_S(PO_2)^-$ contribution only (solid lines). For $w_0 = 1$, the measured peaks at low and high frequency are relatively well separated, allowing for a reliable adjustment of the model parameters (Table S1, SI). The remaining deviations in the outer wings of the calculated frequency slices for both $\nu_{AS}(PO_2)^-$ and $\nu_S(PO_2)^-$ are mainly due to the overlap of neighboring, partly weaker peaks in the experimental 2D spectra, an effect not included in the calculations.

The antidiagonal cuts (solid lines in Figure 3b,d) are determined by the difference of the spectrally overlapping (positive) $\nu = 0$ to 1 and the (negative) $\nu = 1$ to 2 2D envelopes. The two individual envelopes (not shown) are close

dx.doi.org/10.1021/jz402493b | J. Phys. Chem. Lett. 2014, 5, 506−511

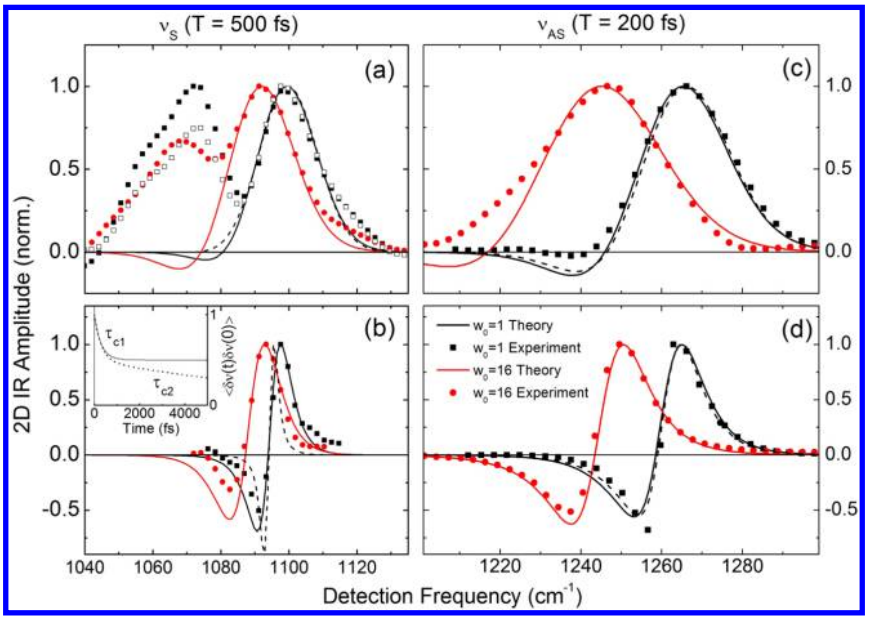

Figure 3. (a) Frequency slices through the $v = 0$ to 1 contribution of the 2D spectra (yellow–red contours in Figure 2) (population time $T = 500$ fs) parallel to the diagonal $\nu_1 = \nu_3$ (solid symbols) for $w_0 = 1$ and 16. The signals above 1080 cm^{-1} represent the diagonal $\nu_S(PO_2)^-$ peak. The signals at low detection frequencies originate from the diagonal peak of the symmetric CO–O–C and C–O–P stretch vibrations centered at 1068 cm^{-1}. Open symbols: Slice for a population time of 2000 fs ($w_0 = 1$). Solid lines: Frequency cuts derived from theoretical 2D spectra calculated with the parameters given in the SI. Dashed line: calculation without the 300 fs component in the tcf. (b) Frequency slices of the 2D spectra of $\nu_S(PO_2)^-$ along an antidiagonal through the frequency position (1093,1096) cm^{-1} for $w_0 = 1$ and (1088,1092) cm^{-1} for $w_0 = 16$ (symbols) together with calculated cuts (solid lines). The dashed line gives a slice that was calculated without the 300 fs component in the tcf, illustrating that this fast component is essential to fit the experimental antidiagonal width of $\nu_S(PO_2)^-$. (Inset) Schematic tcf consisting of two components of the same amplitude with decay times τ_{c1} and τ_{c2}. Dashed–dotted line: $\tau_{c1} = 300$ fs, $\tau_{c2} = 10$ ps; solid line: $\tau_{c1} = 300$ fs, $\tau_{c2} \rightarrow \infty$. (c,d) Same for the 2D spectra of $\nu_{AS}(PO_2)^-$ (population time $T = 200$ fs). The antidiagonal cuts cross the points (1257,1270) cm^{-1} for $w_0 = 1$ and (1236,1251) cm^{-1} for $w_0 = 16$.

to Lorentzian in shape with a nearly identical spectral width of ~17 cm^{-1} (fwhm of $\nu_{AS}(PO_2)^-$ at $w_0 = 1$) that is substantially larger than the anharmonicity of ~5 cm^{-1}. The spectral width is determined by both the population decay time of the $v = 1$ state of the oscillators and the fast decay of the tcf with $\tau_{c1} = 300$ fs. For $\nu_{AS}(PO_2)^-$, the 300 fs population decay makes the main contribution to the line width, while the tcf decay is less relevant (solid and dashed lines in Figure 3d). In contrast, the fast tcf decay is indispensable in order to account for the experimental antidiagonal width of $\nu_S(PO_2)^-$ (symbols and solid line in Figure 3b). A frequency cut calculated with just the contribution from the 1–1.5 ps population decay of $\nu_S(PO_2)^-$ (dashed line in Figure 3b) is much narrower than the measured one. Thus, the $\nu_S(PO_2)^-$ 2D spectra indicate the presence of the fast 300 fs component in the tcf.

The slow component in the tcf is required to account for the pronounced inhomogeneous broadening of the 2D spectra and their minor reshaping, that is, minor spectral diffusion with increasing population time T. A value of $\tau_{c2} \rightarrow \infty$ corresponds to a constant second component in the tcf (solid line in the inset of Figure 3b). The fact that spectral diffusion is practically absent allows one to set a lower limit of $\tau_{c2} > 10$ ps. This is evident from the 2D spectra calculated with $\tau_{c2} = 10$ ps and discussed in the SI (Figure S6). Such calculated 2D spectra exhibit a significant reshaping of the 2D envelopes and CLs, in clear disagreement with the experimental results.

We now discuss the physical processes and molecular interactions determining the structural dynamics of the water–phospholipid interface. The phospholipid surface displays substantial structural disorder with different local phosphate geometries and local electric field distributions. This disorder is clearly manifested in the substantial inhomogeneous broadening of $\nu_S(PO_2)^-$ and $\nu_{AS}(PO_2)^-$ 2D spectra recorded at $w_0 = 1$, that is, very low water content. It is also present in the linear infrared spectra, as is evident from a comparison with the calculated vibrational absorption bands in Figure S7 (SI). Fluctuating electric fields originating from motions of the charged phospholipid head groups and, at higher hydration levels, structural fluctuations of the hydrogen bond pattern at the interface generate a fluctuating force that acts on the $\nu_S(PO_2)^-$ and $\nu_{AS}(PO_2)^-$ oscillators and changes their transition frequencies as a function of time. This mechanism leads to a decay of the tcf with time constants characteristic for the underlying molecular motions.

In the tcf's derived from the 2D spectra, the initial 300 fs decay component is found to contribute even at the very low hydration level of $w_0 = 1$, where individual water molecules interact with either the phosphate or carbonyl groups of DOPC.[9,11] According to our calculations (cf. Table S1, SI), the amplitude of this component increases by only 30% for the fully hydrated DOPC molecules ($w_0 = 16$). We conclude that the initial decay is dominated by fluctuations of the DOPC head groups at the interface rather than by water fluctuations.

Experiments and MD simulations have shown that the dipole formed by the phospholipid phosphate and choline groups with a value of up to 20 D is tilted by an angle of approximately 70° relative to the interface normal and generates strong electric fields in the interface plane.[6,7,9−11] Such fields determine the local arrangement of neighboring DOPC dipoles and orient the much smaller water dipoles (1.85 D) in a way that they partly compensate for the DOPC dipoles. Fluctuations of the DOPC dipole arrangement lead to a fluctuating electric force that is felt

dx.doi.org/10.1021/jz402493b | J. Phys. Chem. Lett. 2014, 5, 506–511

by the $\nu_S(PO_2)^-$ and $\nu_{AS}(PO_2)^-$ oscillators located at the negatively charged end of a head group dipole. We attribute the 300 fs decay of the tcf mainly to this mechanism and consider low-frequency motions in the range of 100 cm^{-1}, such as molecular breathing motions,[32] to be the relevant DOPC physical degrees of freedom. The amplitude increase of this fast tcf component at high hydration levels points to a limited additional contribution of the phosphate water shell. While the orientation of the water dipoles is still governed by the strong DOPC electric field, water molecules can undergo angular fluctuations within existing hydrogen bonds with DOPC. This "wobbling in a cone" has been invoked to explain the limited fast decay of pump−probe anisotropy in experiments where the OD stretch vibration of HOD molecules interacting with phospholipid membranes has been studied.[19,22,23] It is interesting to note that at high hydration levels, fluctuations of the inner water pool of the DOPC reverse micelles have a minor influence on the tcf of the phosphate stretch vibrations. This fact points to a fluctuating force from the water pool that is substantially weaker than the DOPC electric forces and partly screened by the interfacial water molecules.

The pronounced inhomogeneous broadening of the $\nu_S(PO_2)^-$ and $\nu_{AS}(PO_2)^-$ 2D spectra persists with very minor changes up to population times T on the order of 5 ps (for $\nu_S(PO_2)^-$) and is accounted for by the slow component of the tcf, which decays with $\tau_{c2} > 10$ ps. The absence of spectral diffusion on this time scale shows that the exchange dynamics of local phospholipid geometries is slow, corresponding to a "static" structural disorder independent of the level of hydration. Moreover, the local interaction geometries at the fully hydrated interface ($w_0 = 16$) with water−phosphate hydrogen bonds are essentially preserved. Hydrogen bond breaking and re-formation events as well as changes in the water−phosphate coordination number would result in pronounced spectral jumps, that is, spectral diffusion, of the phosphate stretch frequencies (cf. Figure 1b). We, thus, consider the tcf decay time $\tau_{c2} > 10$ ps to be a lower limit for both the lifetime of water−phosphate hydrogen bonds and the water residence time in the interfacial layer. Our results serve as a benchmark for comparison with MD simulations, which display a substantial spread of calculated time constants.

In conclusion, we have mapped fluctuating structural dynamics of water−phospholipid interfaces by measuring infrared 2D spectra of the symmetric and asymmetric phosphate stretch vibrations. In contrast to studies of water vibrations, this new approach addresses the interfacial dynamics much more selectively, even at biologically relevant high hydration levels. We observe structural fluctuations of the phospholipid dipole geometries in the interfacial layer on a 300 fs time scale, whereas the water−phosphate hydrogen bond pattern persists for longer than 10 ps. We envisage the application of dynamic phosphate stretching probes in a wide range of biomolecules.

EXPERIMENTAL METHODS

A short description of the preparation of reverse micelles is given in the SI. The 2D infrared spectra were derived from heterodyne-detected three-pulse photon echoes,[26,27] where three pulses of approximately 100 fs duration interact sequentially with the DOPC sample and a fourth pulse serves as a local oscillator for heterodyning the photon echo signal in a phase-resolved detection scheme. Details of the pulse generation scheme, the photon echo experiment, and the data analysis are given in the SI. All measurements have been performed with samples at a temperature of 300 K.

ASSOCIATED CONTENT

Supporting Information

Details about the preparation of DOPC reverse micelles, the setup for acquisition of 2D spectra, pump−probe data of the symmetric phosphate stretching vibration, cuts through the 2D spectra, normalized 2D spectra and frequency cuts, a description as well as results of the calculations of 2D spectra, and a comparison of calculated and experimental linear vibrational spectra. This material is available free of charge via the Internet at http://pubs.acs.org.

AUTHOR INFORMATION

Corresponding Author

*E-mail: elsasser@mbi-berlin.de. Phone: +49 30 63921400. Fax +49 30 63921409.

Notes

The authors declare no competing financial interest.

ACKNOWLEDGMENTS

The research leading to these results has received funding from the European Research Council under the European Union's Seventh Framework Programme (FP7/2007-2013)/ERC Grant Agreement No. 247051.

REFERENCES

(1) Saenger, W.; Hunter, W. H.; Kennard, O. DNA Conformation is Determined by Economics in the Hydration of Phosphate Groups. *Nature* **1986**, *324*, 385−388.

(2) Wiener, M. C.; White, S. H. Structure of a Fluid Dioleoylphosphatidylcholine Bilayer Determined by Joint Refinement of X-ray and Neutron Diffraction Data. *Biophys. J.* **1992**, *61*, 434−447.

(3) Gawrisch, K.; Gaede, H. C.; Mihailescu, M.; White, S. H. Hydration of POPC Bilayers Studied by ^{1}H-PFG-MAS-NOESY and Neutron Diffraction. *Eur. Biophys. J.* **2007**, *36*, 281−291.

(4) Tobias, D. J.; Tu, K.; Klein, M. L. Atomic Scale Molecular Dynamics Simulations of Lipid Membranes. *Curr. Opin. Colloid Interface Sci.* **1997**, *2*, 15−26.

(5) Gawrisch, K.; Ruston, D.; Zimmerberg, J.; Parsegian, V. A.; Rand, R. P.; Fuller, N. Membrane Dipole Potentials, Hydration Forces, and the Ordering of Water at Membrane Surfaces. *Biophys. J.* **1992**, *61*, 1213−1223.

(6) Chen, X.; Hua, W.; Huang, Z.; Allen, H. C. Interfacial Water Structure Associated with Phospholipid Membranes Studied by Phase-Sensitive Vibrational Sum Frequency Generation Spectroscopy. *J. Am. Chem. Soc.* **2010**, *132*, 11336−11342.

(7) Foglia, F.; Lawrence, M. J.; Lorenz, C. D.; McLain, S. E. On the Hydration of the Phosphocholine Headgroup in Aqueous Solution. *J. Chem. Phys.* **2010**, *133*, 145103.

(8) Alper, H. E.; Bassolino-Klimas, D.; Stouch, T. R. The Limiting Behavior of Water Hydrating a Phospholipid Monolayer: A Computer Simulation Study. *J. Chem. Phys.* **1993**, *99*, 5547−5559.

(9) Pasenkiewicz-Gierula, M.; Takaoka, Y.; Miyagawa, H.; Kitamura, K.; Kusumi, A. Hydrogen Bonding of Water of Phosphatidylcholine in the Membrane as Studied by a Molecular Dynamics Simulation: Location, Geometry, and Lipid−Lipid Bridging via Hydrogen-Bonded Water. *J. Phys. Chem. A* **1997**, *101*, 3677−3691.

(10) Shinoda, W.; Shimizu, M.; Okazaki, S. Molecular Dynamics Study on Electrostatic Properties of a Lipid Bilayer: Polarization, Electrostatic Potential, and the Effects on Structure and Dynamics of Water near the Interface. *J. Phys. Chem. B* **1998**, *102*, 6647−6654.

(11) Saiz, L.; Klein, M. L. Structural Properties of a Highly Polyunsaturated Lipid Bilayer from Molecular Dynamics Simulations. *Biophys. J.* **2001**, *81*, 204−218.

(12) Saiz, L.; Klein, M. L. Electrostatic Interactions in a Neutral Model Phospholipid Bilayer by Molecular Dynamics Simulations. *J. Chem. Phys.* **2002**, *116*, 3052−3057.
(13) Bhide, S. Y.; Berkowitz, M. L. Structure and Dynamics of Water at the Interface with Phospholipid Bilayers. *J. Chem. Phys.* **2005**, *123*, 224702.
(14) Venable, R. M.; Zhang, Y.; Hardy, B. J.; Pastor, R. W. Molecular Dynamics Simulations of a Lipid Bilayer and of Hexadecane: An Investigation of Membrane Fluidity. *Science* **1993**, *262*, 223−226.
(15) König, S.; Sackmann, E.; Richter, D.; Zorn, R.; Carlile, C.; Bayerl, T. M. Molecular Dynamics of Water in Oriented DPPC Multilayers Studied by Quasielastic Neutron Scattering and Deuterium-Nuclear Magnetic Resonance Relaxation. *J. Chem. Phys.* **1994**, *100*, 3307−3316.
(16) Tarek, M.; Tobias, D. J.; Chen, S. H.; Klein, M. L. Short Wavelength Collective Dynamics in Phospholipid Bilayers: A Molecular Dynamics Study. *Phys. Rev. Lett.* **2001**, *87*, 238101.
(17) Mondal, J. A.; Nihonyanagi, S.; Yamaguchi, S.; Tahara, T. Three Distinct Water Structures at a Zwitterionic Lipid/Water Interface Revealed by Heterodyne-Detected Vibrational Sum Frequency Generation. *J. Am. Chem. Soc.* **2012**, *134*, 7842−7850.
(18) Volkov, V. V.; Palmer, D. J.; Righini, R. Heterogeneity of Water at the Phospholipid Membrane Interface. *J. Phys. Chem. B* **2007**, *111*, 1377−1383.
(19) Zhao, W.; Moilanen, D. E.; Fenn, E. E.; Fayer, M. D. Water at the Surfaces of Aligned Phospholipid Multibilayer Model Membranes Probes with Ultrafast Vibrational Spectroscopy. *J. Am. Chem. Soc.* **2009**, *130*, 13927−13937.
(20) Costard, R.; Levinger, N. E.; Nibbering, E. T. J.; Elsaesser, T. Ultrafast Vibrational Dynamics of Water Confined in Phospholipid Reverse Micelles. *J. Phys. Chem. B* **2012**, *116*, 5752−5759.
(21) Costard, R.; Greve, C.; Heisler, I. A.; Elsaesser, T. Ultrafast Energy Redistribution in Local Hydration Shells of Phospholipids: A Two-Dimensional Infrared Study. *J. Phys. Chem. Lett.* **2012**, *3*, 3646−3651.
(22) Zhang, Z.; Berkowitz, M. L. Orientational Dynamics of Water in Phospholipid Bilayers with Different Hydration Levels. *J. Phys. Chem. B* **2009**, *113*, 7676−7680.
(23) Gruenbaum, S. M.; Skinner, J. L. Vibrational Spectroscopy of Water in Hydrated Lipid Multi-bilayers. I. Infrared Spectra and Ultrafast Pump−Probe Observables. *J. Chem. Phys.* **2011**, *135*, 075101.
(24) Levinger, N. E.; Costard, R.; Nibbering, E. T. J.; Elsaesser, T. Ultrafast Energy Migration Pathways in Self-Assembled Phospholipids Interacting with Confined Water. *J. Phys. Chem. A* **2011**, *115*, 11952−11959.
(25) Levinson, N. M.; Bolte, E. E.; Miller, C. S.; Corcelli, S. A.; Boxer, S. G. Phosphate Vibrations Probe Local Electric Fields and Hydration in Biomolecules. *J. Am. Chem. Soc.* **2011**, *133*, 13236−12239.
(26) Asplund, M. C.; Zanni, M. T.; Hochstrasser, R. M. Two-Dimensional Infrared Spectroscopy of Peptides by Phase-Controlled Femtosecond Vibrational Photon Echoes. *Proc. Natl. Acad. Sci. U.S.A.* **2000**, *97*, 8219−8224.
(27) Mukamel, S. Multidimensional Femtosecond Correlation Spectroscopies of Electronic and Vibrational Excitations. *Annu. Rev. Phys. Chem.* **2000**, *51*, 691−729.
(28) Khalil, M.; Demirdöven, N.; Tokmakoff, A. Coherent 2D IR Spectroscopy: Molecular Structure and Dynamics in Solution. *J. Phys. Chem. A* **2003**, *107*, 5258−5279.
(29) Jackson, M.; Mantsch, H. H. Biomembrane Structure from FT-IR Spectroscopy. *Spectrochim. Acta* **1993**, *15*, 53−69.
(30) Kwak, K.; Park, S.; Finkelstein, I. J.; Fayer, M. D. Frequency−Frequency Correlation Functions and Apodization in Two-Dimensional Infrared Vibrational Echo Spectroscopy: A New Approach. *J. Chem. Phys.* **2007**, *127*, 124503.
(31) Hamm, P.; Zanni, M. *Concepts and Methods of 2D Infrared Spectroscopy*; Cambridge University Press: Cambridge, U.K., 2011; Chapter 7.
(32) Hielscher, R.; Hellwig, P. Specific Far Infrared Spectroscopic Properties of Phospholipids. *Spectroscopy* **2012**, *27*, 525−532.